Mitigating Energy Cost of Connection Reliability in UWSNs Through Non-uniform k-Connectivity

Cagla Tantur Karagul, Mehmet Burak Akgun, Huseyin Ugur Yildiz, *Senior Member, IEEE*, and Bulent Tavli, *Senior Member, IEEE*

***Abstract*—Underwater sensing via networked platforms (i.e., underwater wireless sensor networks – UWSNs) is extremely useful in a plethora of applications such as monitoring underwater assets and surveillance against submerged threats. Maintaining reliable connectivity is of utmost importance in UWSNs, which can be achieved through *k*-connectivity (i.e., each sensor node maintains at least *k* node-disjoint paths towards the base station – BS). However, the energy cost of *k*-connectivity is prohibitively high, especially with large *k* values. As a tradeoff, it is possible to mitigate the extra energy cost of *k*-connectivity by employing a non-uniform *k* assignment strategy in a UWSN (e.g., only the most critical sensors have high *k* values whereas the rest of the nodes have lower *k* values). Non-uniform *k*-connectivity is a novel concept which has never been systematically investigated in the literature, to the best of our knowledge. In this study, we investigate the tradeoff between network lifetime (NetL) and reliability via non-uniform *k*-connectivity through the use of a novel optimization framework. Our analysis reveal that it is possible to provide strong connection reliability to critical nodes by adopting a non-uniform *k*-connectivity strategy without deteriorating network lifetime significantly.**

***Index Terms*—underwater wireless sensor networks, k-connectivity, network lifetime, mixed-integer linear programming, reliability.**

I. Introduction

OCEANS, seas, lakes, rivers, and other bodies of water constitute the majority of the surface of our planet, making monitoring of aquatic environments essential for various purposes, including coastal studies, underwater defense operations, fish farming, and ongoing pollution tracking [1]. Advances in communication technologies, particularly underwater acoustic systems, have matured enough to make underwater wireless sensor networks (UWSNs) practical and effective for scientific, industrial, and defense uses since the beginning of the twenty-first century [2]. A UWSN comprises multiple sensor nodes, floating or submerged, spread across a region to track environmental factors such as temperature, pressure, and humidity. These networks include at least one base station (BS), which can be positioned at a specific depth or on the surface of the water to collect data from the sensor nodes. Initially, UWSNs relied on single-hop communication, where sensors sent data directly to the BS. However, with technological progress, multi-hop communication has become the preferred method, offering benefits such as broader coverage, improved energy efficiency, and greater reliability [3].

For UWSNs, two paramount concerns are the efficient management of energy resources and the reliability of network operations [4]. Given that sensor nodes rely on finite battery supplies that are typically difficult or unfeasible to replenish, it is crucial to cut energy expenditure. Concurrently, the network's resilience is of utmost importance because the harsh underwater conditions can lead to disruptions in node functionality and communication links. The most common definition of a k-connected network is that each node in the network has k node-disjoint paths to all to the other nodes [5]. However, in this study, we opt to utilize the definition where each sensor node in the network has at least k node-disjoint paths to the BS, which suits well with the typical use cases of wireless sensor networks (WSNs) [6]. As such, a network designed with k-connectivity guarantees that every sensor node has no fewer than k node-disjoint routes to the BS. This architectural approach fortifies the network's resilience, especially with a high k value, by maintaining connectivity even if as many as $k-1$ nodes become inoperable.

Ensuring a k-connected UWSN demands additional power to sustain at least k separate routes from each sensor node to the base station. This creates a balance to strike between the degree of dependability, determined by the k value, and the operational duration of the network, known as network lifetime (NetL). The literature on the exploration of the impact of k-connectivity on NetL in UWSNs is scarce [6], [7]. The results presented in [6] reveals that preserving k-connectivity can cause a considerable reduction in NetL. To mitigate the prohibitively high energy cost of uniform k-connectivity (i.e., all sensor nodes maintain k disjoint paths to the BS) throughout a UWSN, in this study, we propose the novel concept of non-uniform k-connectivity. In certain UWSN applications not all the sensor nodes are required to have the highest reliability level (i.e., only a critically important subset of the sensor nodes needs to maintain the highest k value) [5]. Hence, it is possible to provide a plurality of reliability levels through a non-uniform k assignment strategy, which has a potential to curtail the energy cost of uniform k-connectivity in UWSNs.

The problem statement, its urgency, and the significance of the research approach is clearly articulated as follows. The importance of UWSNs is increasing due to the ever-growing interest in underwater environment, globally, which gives rise to the need to monitor the underwater environment efficiently.

C. Tantur Karagul and B. Tavli are with the Department of Electrical and Electronics Engineering, TOBB University of Economics and Technology, 06560, Ankara, Turkey. (e-mail: {ckaragul,btavli}@etu.edu.tr).

M. B. Akgun is with the Department of Computer Engineering, TOBB University of Economics and Technology, 06560, Ankara, Turkey. (e-mail: m.akgun@etu.edu.tr).

H. U. Yildiz is with the Department of Electrical and Electronics Engineering, TED University, 06420, Ankara, Turkey (e-mail: hugur.yildiz@tedu.edu.tr).

UWSNs are among the most effective underwater monitoring and sensing technologies. Due to the limited battery energies of the sensor nodes, energy-efficient operation of UWSNs is of utmost importance. Effective monitoring of the underwater environment via UWSNs requires connection reliability of the network. k-connectivity is a prominent approach to achieve connection reliability. However, k-connectivity, especially with high k values deteriorates NetL of a UWSN. As a remedy to this problem we propose non-uniform k-connectivity in UWSNs. To be able to analyze the potential benefits brought by non-uniform k-connectivity under optimal conditions, we created a novel mixed-integer linear programming (MILP) framework, which is employed to characterize the energy dissipation characteristics of non-uniform k-connectivity in UWSNs.

The novel contributions of this study are threefold, which are enumerated as follows:

1) We thoroughly explore the impact of non-uniform k-connectivity on energy consumption and network lifetime in UWSNs, which is a problem previously unaddressed in existing studies, to the best of our knowledge.
2) We create a novel optimization framework based on MILP that is capable of modeling UWSN energy dissipation as well as non-uniform k-connectivity.
3) We characterize the interplay between NetL and reliability level provided under ideal yet practical settings for a wide range of parameters through the solutions of the optimization model.

The structure of this paper is as follows. Section II offers a brief overview of prior work on k-connectivity and NetL, highlighting the unique contributions of this research compared to existing studies. Section III introduces the system model, including the network structure, energy consumption model, and optimization framework. The findings based on the solutions of the optimization problems with a rich set of parameters are elaborated in Section IV. The key conclusions of this study are summarized in Section V.

II. Related Work

Studies on the resilience of WSN connectivity can be divided into three main areas: node placement, connectivity reestablishment, and connectivity assessment. Research on node placement generally focuses on developing techniques or configurations to facilitate connected topology creation [8], [9], optimize coverage [10], [11], or prolong NetL [12], [13]. Key placement approaches include positioning nodes at designated spots [9], [14] and adjusting node transmission power levels [15], [16] to achieve k-connectivity. While placing nodes at specific locations can enable an effective k-connected network, this strategy is often impractical in challenging or irregular terrains [17]. Boosting the transmission power of sensor nodes can create more connections, aiding in forming a k-connected network with the desired connectivity level, but this approach increases energy use and can shorten NetL [7].

The initial phase of any algorithm focused on k-connectivity involves assessing or approximating the network's k value [18], [19]. Determining a network's k value is a classic challenge in graph theory, tackled through various sequential [20] and distributed algorithms [21]–[23]. Identifying the k value can yield critical insights into the network's fault tolerance and dependability. A study on the reliability of k-connectivity in underwater optical wireless networks is detailed in [24], examining factors like data rate, wavelength, error rates, transmission power, and node density. Most research on connectivity restoration offers effective methods to recover diminished or lost connectivity following node or link failures [25], [26]. When a failure reduces a network's k value, connectivity can be restored to the target level by strategically deploying new sensor nodes or repositioning existing ones to optimal locations.

NetL is widely regarded as a critical measure of performance in WSNs. Equally vital, particularly for underwater networks, is ensuring dependable network functionality [3]. Preserving k-connectivity is an effective strategy for securing reliable network links, especially with higher k values. Yet, much of the research on k-connectivity (spanning deployment, detection, and restoration) centers on 1-connectivity (i.e., $k = 1$). Maintaining robust connectivity remains a key hurdle in WSNs, explored extensively from various angles. In [27], a probabilistic k-coverage algorithm is introduced to extend NetL by ensuring a grid of target points is monitored by randomly placed WSN nodes. Here, k-coverage means each target point is observed by at least k operational (non-sleeping) nodes, with these active nodes configured to stay interconnected. However, this study focuses exclusively on achieving 1-connectivity rather than broader k-connectivity ($k > 1$).

In fact, there are only two studies in the literature which investigate both the k value and lifetime in sensor networks, jointly [6], [7]. In [7], two cases are investigated for terrestrial WSNs: (i) the maximum transmission power level is used for all sensor nodes, which causes occupation of the highest possible k value of the network and (ii) transmission power levels that maximize the network lifetime is used. Comparative evaluation of the two cases reveals that the first case results in approximately up to 35% reduction of network lifetime and up to 20% increase in the k value when compared to the second case. However, apart from the two extreme cases, there is no other characterization of the interaction between k-connectivity and network lifetime. In [6], the interplay between NetL and k value of a UWSN is investigated by utilizing an optimization framework. It is shown that NetL can decrease significantly for high k values. This study is important because it is the first study that characterizes the energy cost of uniform k-connectivity in UWSNs. However, the optimization model proposed in [6] does not account for the energy cost of control packet transmissions for the maintenance of the paths and non-uniform k-connectivity is not addressed.

To contribute to this unexplored area in the literature, in this study, we present an optimization framework, which is capable of maximizing UWSN lifetime for arbitrary k value assignments (i.e., non-uniform k-connectivity) to the sensor nodes. Using the developed optimization framework, we examine a broad range of parameters to quantitatively and systematically inspect the interplay between non-uniform k-

connectivity and NetL in UWSNs, as of our knowledge, this has not been addressed in the existing literature.

III. System Model

This section presents our system model, comprising the network model (Subsection III-A), the underwater energy consumption model (Subsection III-B), and the MILP-based optimization framework (Subsection III-C). Table I summarizes the terminology employed in this study.

A. Network Model

We consider an underwater environment in the shape of a rectangular prism. The dimensions of this rectangular prism are labeled as d_x, d_y, and d_z, representing the width, length, and depth, respectively (in km). The network consists of multiple sensor nodes (represented by set $\mathcal{W}$) deployed according to the random uniform distribution within the rectangular prism-shaped region. Furthermore, a single static BS is located at one of the top four corners of the network deployment volume, functioning as a sonobuoy. Sensor nodes are anchored to fixed positions to remain stationary during operation. Sensor nodes periodically generate data packets (encapsulating the data they sense) and transmit them to the sonobuoy.

The network is abstracted as a directed graph, $\mathcal{G} = (\mathcal{V}, \mathcal{A})$. Here, $\mathcal{V}$ represents the set of all nodes (including the BS) in the network, and $\mathcal{A} = \{(i,j) : i \in \mathcal{V},\ j \in \mathcal{V} \setminus \{i\}, d_{ij} \leq \mathcal{R}_{\max}(\ell_{\max})\}$ denotes the set of all links in the network. The transmission power level is adjusted based on the distance between the transmitter and receiver nodes. We assume ten transmission power levels defined as the set $\mathcal{P}_\ell = \{1, 2, \ldots, 10\}$, where $\mathcal{R}_{\max}(\ell)$ denotes the utmost distance over which transmission can occur when the power level-ℓ is being used. The maximum transmission level is defined as $\ell_{\max} = 10$. Therefore, a link between node-i and node-j can be established if the distance between them (i.e., d_{ij}) is less than or equal to the maximum transmission range, $\mathcal{R}_{\max}(\ell_{\max})$.

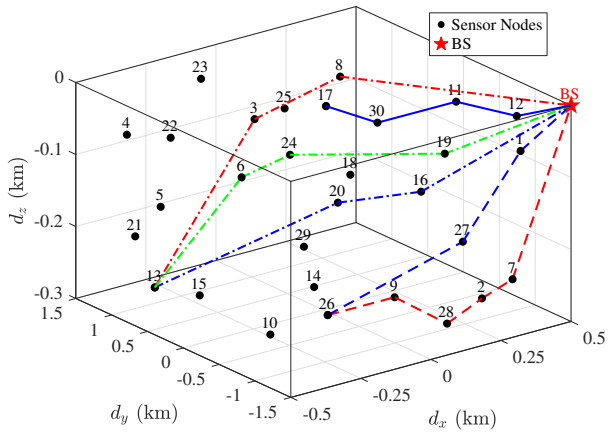

Fig. 1: 3D view of the UWSN topology. The BS is marked with a red star. Paths from three selected sensor nodes (node-13, node-17, and node-26) to the BS are shown with colored lines: blue (path-1), red (path-2), and green (path-3).

Fig. 1 illustrates a sample 3D UWSN deployment within a rectangular prism-shaped environment with dimensions $d_x =$ 1 km, $d_y = 3$ km, and $d_z = 0.3$ km. 30 sensor nodes ($|\mathcal{W}| =$ 30) are randomly distributed throughout this volume, while a single BS is positioned at one of the prism's top corners (marked with a red star).

The operational lifetime of the network is partitioned into rounds of equal duration, with each round lasting $t_r = 300$ s. The network is assumed to be operational for $N_r = 1440$ rounds. Each sensor node generates a single data packet (i.e., $s_k = 1$) of 1024 bits (i.e., $l_d = 1024$ bits) during a single round. Furthermore, every sensor node sends control packets on each one of its active paths towards the BS. The control packet size is 256 bits (i.e., $l_c = 256$ bits). The relative frequency of the control packets with respect to the data packet generation frequency is defined by the parameter ξ (e.g., if $\xi =$ 4 then four control packets are sent within the time frame that one data packet is sent).

Control packets are, typically, utilized for link and path maintenance in communication protocols. In our framework, control packets are employed as an abstraction to account for operational overhead of networking mechanisms in terms of energy consumption and bandwidth utilization.

The data packets generated by each sensor node are transmitted to the BS via either single-hop or multi-hop communications. Every sensor node possesses a minimum of κ_n distinct routes to the BS, indicating κ_n-connectivity. The value of κ_n is exclusively determined for each subset $\mathcal{W}_n$ of sensor nodes.

B. Energy Consumption Framework

The energy dissipation model presented in [28] is utilized in this paper. The transmission loss over the distance $\mathcal{R}_{\max}(\ell)$, is calculated as follows

$$TL(\mathcal{R}_{\max}(\ell)) = \mathcal{R}_{\max}(\ell)^{k_s} \times \nu^{10^{-3}\mathcal{R}_{\max}(\ell)}, \tag{1}$$

where $k_s = 1.5$, $\nu = 10^{\alpha(f_0)/10}$, $\alpha(f_0)$, and $f_0 = 25$ KHz represent the spreading factor, the frequency-dependent component, the absorption coefficient, and operating frequency respectively. The absorption coefficient is derived with Thorp's formula as

$$\alpha(f_0) = \frac{0.11 f_0^2}{1+f_0^2} + \frac{44 f_0^2}{4100+f_0^2} + 2.75 \cdot 10^{-4} f_0^2 + 0.003. \tag{2}$$

Assuming that the desired energy level at the receiver's input is $P_0 = 1\times$ 10^{-7} J/bit [28], the energy required to transmit a single bit using transmission power level-ℓ is obtained as

$$\mathcal{E}_T(\ell) = TL(\mathcal{R}_{\max}(\ell)) \times P_0. \tag{3}$$

The energy cost for receiving a single bit is defined as

$$\mathcal{E}_R = P_r, \tag{4}$$

where $P_r = 0.2 \times$ 10^{-7} J/bit is the reception constant [28].

The transmission energies calculated using ten transmission powers and corresponding ten transmission ranges are presented in Table II. Each node adjusts its transmission power based on the distance between the transmitter and receiver nodes. The mapping between the transmission energy and

TABLE I: The set of symbols and terms utilized in this study.

Symbol	Description	Unit	Value	Symbol	Description	Unit	Value
$\mathcal{A}$	Set of all links	–	–	d_{ij}	Distance between node-i and node-j	m	–
(d_x, d_y, d_z)	Width, length, and depth of the network	km	(1,1–3, 0.30)	$\mathcal{E}_R = P_r$	Reception constant	J/bit	0.2×10^{-7}
$\mathcal{E}_T(\ell)$	Energy cost of transmission using the power level-ℓ	mJ/bit	–	$\mathcal{E}^*_{T,ij}$	Optimum transmission energy for transmission over the link-(i,j)	mJ/bit	–
f_0	Center of operating frequency	KHz	25	f^{kl}_{ij}	Number of data packets (each of size l_d bits) generated by node-k, flowing over the link-(i,j) on path-l	packets	–
$\mathcal{G}$	Network graph	–	–	g^{kl}_{ij}	Number of control packets (each of size l_c bits) generated by node-k, flowing over the link-(i,j) on path-l	packets	–
h^{kl}_{ij}	Binary variable that shows whether the data generated by node-k on the path-l flows over the link-(i,j) or not	–	–	$\mathcal{I}^i_{jm}$	Interference parameter	–	–
k_s	Spreading factor	–	1.5	l_c	Control packet size	bits	256
l_d	Data packet size	bits	1024	M	Sufficiently large number	–	10^4
$\ell_{\max}$	Maximum power level	–	10	N_r	Total number of rounds for network operation	–	1440
P_0	Desired power level at the input to the receiver	J/bit	1×10^{-7}	$\mathcal{P}_\ell$	Set of transmission power levels	–	$\{1, \ldots, 10\}$
p^l_k	Total number of data packets injected into the network by the source node-k on the path-l	packets	–	R_b	Data rate	bps	2500
$\mathcal{R}_{\max}(\ell)$	Maximum transmission range at power level-ℓ	m	$\{100, \ldots, 1000\}$	s_k	Number of packets generated by node-k at each round	–	1
$TL(\mathcal{R}_{\max}(\ell))$	Transmission loss over the distance $\mathcal{R}_{\max}(\ell)$	–	–	t_r	Round duration	s	300
$\mathcal{V}$	Set of all nodes, including the BS	–	–	$\mathcal{W}$	Set of all sensor nodes	–	–
$\alpha(f_0)$	Absorption coefficient	dB/km	–	γ	Interference range multiplier	–	1.7
ε	Total energy dissipated by the most energy-hungry node	J	–	κ_n	The minimum number of disjoint paths required to reach the BS from node-n	–	1–3
ν	Frequency-dependent component for calculating the transmission loss	–	–	ξ	Relative frequency of control packets	–	0.25–4
S_P	The index set of subsets $\mathcal{W}_n$ of sensor nodes that maintain κ_n-connectivity	–	–	N_l	Maximum number of paths	–	5
$\mathcal{W}_n$	The subset of nodes required to have κ_n-disjoint paths to the BS.	–	–	N_f	Number of failed nodes	–	–

TABLE II: Energy consumption for transmission ($\mathcal{E}_T(\ell)$ – mJ/bit) and the range of communication ($\mathcal{R}_{\max}(\ell)$ – m) at power level-ℓ when $f_0 = 25$ KHz and $k_s = 1.5$.

ℓ	$\mathcal{E}_T(\ell)$	$\mathcal{R}_{\max}(\ell)$	ℓ	$\mathcal{E}_T(\ell)$	$\mathcal{R}_{\max}(\ell)$
1	0.115	100	6	3.416	600
2	0.375	200	7	4.954	700
3	0.792	300	8	6.967	800
4	1.404	400	9	9.568	900
5	2.258	500	10	12.897	1000

distance for link-(i,j) is provided for the ten transmission power levels is defined as

$$\mathcal{E}^*_{T,ij} = \begin{cases} \mathcal{E}_T(\ell = 1), \text{ if } d_{ij} \leq \mathcal{R}_{\max}(\ell = 1) \\ \infty, \text{ if } d_{ij} > \mathcal{R}_{\max}(\ell = 10) \\ \mathcal{E}_T(\ell + 1), \text{ if } \mathcal{R}_{\max}(\ell) < d_{ij} \leq \mathcal{R}_{\max}(\ell + 1) \end{cases}. \tag{5}$$

C. The Optimization Framework

This section introduces our optimization framework that employs MILP methodology for maximizing network lifetime while fulfilling the non-uniform k-connectivity constraints for UWSNs. To maximize the network lifetime, we minimize the energy consumption of the node that dissipates the most energy [29], [30]. The objective function of the MILP model is defined in (6), where ε represents the total energy expended by the most energy consuming sensor node. Note that NetL is inversely proportional to ε [6] (e.g., if ε is doubled then NetL is halved provided that the initial battery energies of all sensor nodes are equal for a given UWSN topology). The constraints of the MILP model are provided in (7)–(25). The decision variables of the MILP model are defined as follows:

- f^{kl}_{ij}: An integer variable that denotes the number of data packets, each of size l_d bits, generated by node-k and flowing over the link-(i,j) on path-l.
- g^{kl}_{ij} is an integer variable that represents the number of control packets, each with a size of l_c bits, that node k generates and sends over link-(i,j) on path l.
- h^{kl}_{ij}: A binary variable representing whether the data generated by node-k on path-l flows over the link-(i,j) or not.
- p^l_k: An integer variable representing the total number of data packets injected into the network by the source node-k on path-l.

Minimize ε (6)

subject to:

$$\sum_{(i,j)\in\mathcal{A}} f^{kl}_{ij} - \sum_{(j,i)\in\mathcal{A}} f^{kl}_{ji} = \begin{cases} p^l_k & \text{if } i = k \\ -p^l_k & \text{if } i = 1 \\ 0 & \text{o.w.} \end{cases}, \quad \forall i \in \mathcal{V},\ k \in \mathcal{W},\ l = \{1, \ldots, N_l\} \tag{7}$$

$$\sum_{l=1}^{N_l} p^l_k = s_k \times N_r, \quad \forall k \in \mathcal{W} \tag{8}$$

$$\sum_{l=1}^{N_l} \sum_{j\in\mathcal{W}} f^{kl}_{jk} = 0, \quad \forall k \in \mathcal{W} \tag{9}$$

$$f^{kl}_{ij} \leq s_k \times N_r \times h^{kl}_{ij}, \quad \forall (i,j) \in \mathcal{A},\ k \in \mathcal{W},\ l = \{1, \ldots, N_l\} \tag{10}$$

$$h^{kl}_{ij} \leq f^{kl}_{ij}, \quad \forall (i,j) \in \mathcal{A},\ k \in \mathcal{W},\ l = \{1, \ldots, N_l\} \tag{11}$$

$$\sum_{(i,j)\in\mathcal{A}} h^{kl}_{ij} \leq 1, \quad \forall i \in \mathcal{W},\ k \in \mathcal{W},\ l = \{1, \ldots, N_l\} \tag{12}$$

$$\sum_{l=1}^{N_l} h_{ij}^{kl} \leq 1, \quad \forall (i,j) \in \mathcal{A},\ k \in \mathcal{W} \tag{13}$$

$$\sum_{(j,1)\in\mathcal{A}} f_{j1}^{k(l+1)} \leq \sum_{(j,1)\in\mathcal{A}} f_{j1}^{kl}, \quad \forall k \in \mathcal{W}, \quad l = \{1,\ldots,N_l - 1\} \tag{14}$$

$$f_{ij}^{kl} - M(1 - h_{ij}^{kl}) \leq p_k^l,\ \ \forall (i,j) \in \mathcal{A},\ k \in \mathcal{W}, \quad l = \{1,\ldots,N_l\} \tag{15}$$

$$f_{ij}^{kl} + M(1 - h_{ij}^{kl}) \geq p_k^l,\ \ \forall (i,j) \in \mathcal{A},\ k \in \mathcal{W}, \quad l = \{1,\ldots,N_l\} \tag{16}$$

$$g_{ij}^{kl} = \xi \times N_r \times (h_{ij}^{kl} + h_{ji}^{kl}),\ \ \forall (i,j) \in \mathcal{A},\ k \in \mathcal{W}, \quad l = \{1,\ldots,N_l\} \tag{17}$$

$$\sum_{(k,j)\in\mathcal{A}} \sum_{l=1}^{N_l} h_{kj}^{kl} \geq \kappa_n, \quad \forall k \in \mathcal{W}_n,\ n \in S_P \tag{18}$$

$$\sum_{(i,j)\in\mathcal{A}} \sum_{l=1}^{N_l} h_{ij}^{kl} \leq 1, \quad \forall\ i \in \mathcal{W} \setminus k, k \in \mathcal{W} \tag{19}$$

$$\sum_{(j,i)\in\mathcal{A}} \sum_{l=1}^{N_l} h_{ji}^{kl} \leq 1, \quad \forall\ i \in \mathcal{W} \setminus k, k \in \mathcal{W} \tag{20}$$

$$\sum_{l=1}^{N_l} \sum_{k\in\mathcal{W}} \sum_{(i,j)\in\mathcal{A}} \mathcal{E}_{T,ij}^{*}(f_{ij}^{kl} l_d + g_{ij}^{kl} l_c) + \sum_{l=1}^{N_l} \sum_{k\in\mathcal{W}} \sum_{(j,i)\in\mathcal{A}} \mathcal{E}_R(f_{ji}^{kl} l_d + g_{ji}^{kl} l_c) \leq \varepsilon,\ \forall i \in \mathcal{W} \tag{21}$$

$$\sum_{k\in\mathcal{W}} \sum_{l=1}^{N_l} \left(\sum_{(i,j)\in\mathcal{A}} \left(f_{ij}^{kl} \frac{l_d}{R_b} + g_{ij}^{kl} \frac{l_c}{R_b} \right) + \sum_{(j,i)\in\mathcal{A}} \left(f_{ji}^{kl} \frac{l_d}{R_b} + g_{ji}^{kl} \frac{l_c}{R_b} \right) + \sum_{(j,m)\in\mathcal{A}\setminus\{i\}} \left(f_{jm}^{kl} \mathcal{I}_{jm}^{i} \frac{l_d}{R_b} + g_{jm}^{kl} \mathcal{I}_{jm}^{i} \frac{l_c}{R_b} \right) \right) \leq N_r \times t_r, \forall i \in \mathcal{V} \tag{22}$$

$$f_{ij}^{kl}, g_{ij}^{kl} \geq 0, \quad \forall (i,j) \in \mathcal{A},\ k \in \mathcal{W},\ l = \{1,\ldots,N_l\} \tag{23}$$

$$h_{ij}^{kl} \in \{0,1\}, \quad \forall (i,j) \in \mathcal{A},\ k \in \mathcal{W},\ l = \{1,\ldots,N_l\} \tag{24}$$

$$p_k^l \geq 0, \quad \forall k \in \mathcal{W},\ l = \{1,\ldots,N_l\} \tag{25}$$

Constraint 7 ensures that the ingress and egress traffic of the BS ($i = 1$), source node-k ($i = k$), and relay node ($i \neq k$) are balanced. In this constraint, p_k^l denotes the total number of data packets injected into the network by the source node-k on path-l. Constraint (8) states that the number of data packets generated by the source node-k during the operational lifespan of the network equals $s_k \times N_r$. Note that the total number of node-disjoint routing paths of each node is upper bounded by N_l. Constraint (9) prohibits the flow of data packets produced by the source node-k and transmitted through the BS back to the source node.

Constraints (10) and (11) specify the value of the binary indicator variable h_{ij}^{kl}, which is one if source node-k's path-l utilizes link-(i,j) otherwise, i.e., if link-(i,j) is not utilized, it is zero. If f_{ij}^{kl} is greater than zero, then h_{ij}^{kl} is equal to one. Conversely, if f_{ij}^{kl} is equal to zero, then h_{ij}^{kl} is equal to zero. Constraint (12) enforces the flow on a given path to have only one next-hop node. In other words, a flow proceeding along a path cannot be divided into several separate paths. Note that paths are not predetermined in the model. However, constraints of the optimization model as a whole ensure that sets of links are optimally determined to form paths. For example, constraint (12) ensures that each path consists of a set of links, which collectively form a non-bifurcated pipeline from a source node to the BS.

Constraint (13) is employed to meet the k-connectivity specifications, ensuring that link-(i,j) is occupied by only one of the paths from the source node-k and that these paths are *link-disjoint*. Constraint (14) guarantees that the quantity of packets produced by the source node-k and routed on the routing path-l diminishes as the value of l grows. This constraint facilitates more convenient analysis of the solutions of the optimization problem instances. Constraints (15) and (16) eliminate any potential phantom flows that could occur, as described in [31]. In these constraints, M is sufficiently large number. Constraint 17 establishes the control packet flow on link-(i,j) based on the control packet frequency, ξ, and the presence of flow on link-(i,j) or link-(j,i). Constraint (18) indicates that the source node-k possesses κ_n paths to the BS, dependent on the set $\mathcal{W}_n$ associated with the source node-k.

S_P is the index set of distinct subsets of nodes. For example, if $|S_P| = 2$ (e.g., $S_P = \{1, 2\}$), then the set of sensor nodes in the network consists of two subsets of sensor nodes (i.e., $\mathcal{W} = \bigcup_{n=1}^{2} \mathcal{W}_n$). In fact, this constraint determines the non-uniform k-connectivity assignment to the sensor nodes. For example, if node-5 is in $\mathcal{W}_2$ set and $\kappa_2 = 2$, then constraint (18) ensures that the optimization problem has a feasible solution only in the case that node-5 is assigned with, at least, two disjoint paths to the BS.

Constraints (19) and (20) are defined to meet k-connectivity requirements by enabling paths to be *node-disjoint*, meaning that any sensor node can only be utilized as a relay in at most one of the paths originating at the source node-k. Each path consists of a set of links (i.e., a chain of links). Through constraints (13), (19), and (20), we make sure that paths of a source node do not share common links or nodes. Hence, paths of a source node are both node-disjoint and link-disjoint.

Constraint (21) computes the energy expended during transmission and reception by node-i, while the MILP model aims to minimize the energy consumption of the node with the highest energy demand. The first triple summation term on the left hand side of the constraint accounts for the energy dissipated for data packet transmissions ($\mathcal{E}_{T,ij}^{*} f_{ij}^{kl} l_d$) and control packet transmissions ($\mathcal{E}_{T,ij}^{*} g_{ij}^{kl} l_c$), including the energy dissipated by the sensor nodes for relaying packets originated at other source sensor nodes (i.e., multi-hop packet traffic). The second triple summation term accounts for data packet receptions ($\mathcal{E}_R f_{ji}^{kl} l_d$) and control packet receptions ($\mathcal{E}_R g_{ji}^{kl} l_c$). In fact, constraint (21) should be satisfied for all

the sensor nodes in the UWSN (i.e., $\forall i \in \mathcal{W}$). Considering one of these constraints with a particular i (e.g., $i = 3$) then the flow variables, f_{ij}^{kl} and g_{ij}^{kl}, can be rewritten as f_{3j}^{kl} and g_{3j}^{kl}. Since we are left with three variables, we need three summations (i.e., $\sum_{l=1}^{N_l} \sum_{k \in \mathcal{W}} \sum_{(i,j) \in \mathcal{A}}$). $\sum_{l=1}^{N_l}$ term is for different paths of a source node. $\sum_{k \in \mathcal{W}}$ term is for different source nodes. $\sum_{(3,j) \in \mathcal{A}}$ term is for the all outgoing links of node-3 considering the transmission energy consumption (all incoming links of node-3 considering the reception energy consumption, i.e., f_{j3}^{kl} and g_{j3}^{kl}).

Constraint (22) restricts the total bandwidth utilization for transmission, reception, and inactivity periods of the node, which arise from the transmissions of proximate nodes, leading to interference. In this constraint, $R_b = 2500$ bps is the data rate and $\mathcal{I}_{jm}^{i}$ is a parameter that equals 1 if node-i is within the interference zone of the communication link between node-j and node-m, and 0 otherwise as defined in Eq. (26).

$$\mathcal{I}_{jm}^{i} = \begin{cases} 1 & \text{if } \gamma d_{jm} \geq d_{ji} \ \forall j \in \mathcal{V}, \ \forall m \in \mathcal{V} \setminus \{j\} \\ 0 & \text{otherwise} \end{cases}, \quad (26)$$

where $\gamma = 1.7$ is the interference range multiplier [32]. In fact, if the minimum transmission power required for node-j to reach node-m plus a certain interference margin exceeds the minimum transmission power required for node-j to reach node-i, which is implied by the condition $\gamma d_{jm} \geq d_{ji}$, then all the data and control packet transmission from node-j to reach node-m results in a significant interference at node-i such that node-i is effectively blocked from data or control packet receptions from any node in the network while node-j transmits to node-m. As such, the third term on the left hand side of constraint (22) accounts for the aggregate bandwidth that each node is depraved off by the packet transmissions of its neighbors. Consider node-3 and the flows between its neighbors node-7 and node-9 (i.e., f_{79}^{kl} and g_{79}^{kl}). If $\gamma d_{79} \geq d_{73}$ then $\mathcal{I}_{79}^{3} = 1$ (i.e., packet flows from node-7 to node-9 creates interference at node-3), which results in reduction of node-3's aggregate bandwidth by aggregate bandwidth due to packet flows from node-7 to node-9.

Finally, Constraints (23), (24), and (25) define the boundaries of the decision variables.

IV. Analysis

In this section, we present our results obtained by solving the MILP model for a wide range of configurations and parameter sets. This allows us to analyze the impact of non-uniform k-connectivity on NetL, which is inversely proportional to ε. We first analyze the impact of the relative frequency of control packets, ξ, on ε in Subsection IV-A. Detailed analysis of a particular UWSN topology is presented in Subsection IV-B, which is especially instructive in assessing the dynamics of non-uniform k-connectivity in UWSNs. Analysis of larger scale topologies with particularly important κ_n configurations are presented in Subsection IV-C.

We create the network and energy consumption models (Subsections III-A and III-B) using Python and solve the MILP model with GUROBI [33]. The parameters used in the analysis are detailed in Tables I and II. The results presented in Subsections IV-A and IV-C are the averages obtained from 20 independent topologies (i.e., $|\mathcal{W}| = 30$ sensor nodes are deployed randomly) for statistical significance.

Note that this is the first study in the literature that investigates non-uniform k-connectivity concept to the best of our knowledge. Therefore, there is no other proposal in the literature that can be compared to our approach. Nevertheless, we compare the performance of non-uniform k-connectivity with uniform k-connectivity, which, actually, is the most important comparative validation scheme. Furthermore, we create a novel MILP model and solve the model for a rich set of scenarios and a wide parameter space to analyze the characteristics of non-uniform k-connectivity. MILP is an exact mathematical programming-based optimization method. The exact solutions of MILP instances are the optimal solutions under the given settings. Hence, it is not possible to obtain improvements over the optimal solution, thus, there is no point in comparing the optimal solution to any other sub-optimal solution, which, by definition, cannot be better than the optimal solution, for characterization purposes.

A. The Impact of Control Packet Relative Frequency (ξ)

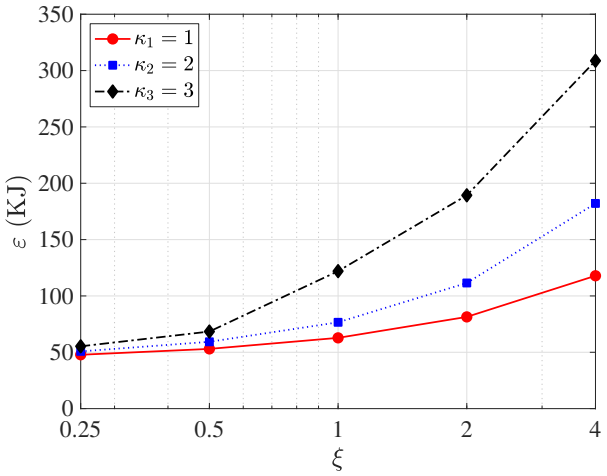

Fig. 2: ε as a function of κ_n (the minimum number of disjoint paths) and ξ (relative frequency of control packets)

Fig. 2 presents ε as a function of the relative frequency of control packets, ξ, for three cases with $d_y = 3$ km. The red curve represents the first case, where all nodes are at least 1-connected (i.e., $\kappa_1 = 1$ and $\mathcal{W} = \mathcal{W}_1$). The blue curve corresponds to second case, where all nodes are at least 2-connected (i.e., $\kappa_2 = 2$ and $\mathcal{W} = \mathcal{W}_2$). The black curve is for the third case, where all nodes are at least 3-connected (i.e., $\kappa_3 = 3$ and $\mathcal{W} = \mathcal{W}_3$). For all values of κ_n, increasing ξ from 0.25 to 4 results in a monotonic increase in ε, which is due to the increased energy burden caused by more frequent control packet transmissions. For example, in third case ε values for $\xi = 0.25$, $\xi = 1$, and $\xi = 4$ are 55.31 KJ, 121.96 KJ, and 308.70 KJ, respectively. Additionally, for any fixed ξ value, ε increases with higher κ_n values, indicating that more robust connectivity (i.e., more path redundancy) comes at the cost of elevated energy consumption. For example, ε values with $\xi =$

TABLE III: k-connectivity configurations.

Scenario	Description
I	All sensor nodes are at least 1-connected to the BS ($\kappa_1 = 1$, $\mathcal{W}_1 = \{1, 2, \ldots, 12\}$), and $\mathcal{W} = \mathcal{W}_1$.
II	Nodes 1–6 are 2-connected ($\kappa_2 = 2$, $\mathcal{W}_2 = \{1, 2, \ldots, 6\}$), nodes 7–12 are 1-connected ($\kappa_1 = 1$, $\mathcal{W}_1 = \{7, 8, \ldots, 12\}$); $\mathcal{W} = \mathcal{W}_1 \cup \mathcal{W}_2$.
III	All sensor nodes are 2-connected ($\kappa_2 = 2$, $\mathcal{W}_2 = \{1, 2, \ldots, 12\}$), and $\mathcal{W} = \mathcal{W}_2$.
IV	Nodes 1–4: $\kappa_1 = 1$; Nodes 5–8: $\kappa_2 = 2$; Nodes 9–12: $\kappa_3 = 3$; $\mathcal{W} = \mathcal{W}_1 \cup \mathcal{W}_2 \cup \mathcal{W}_3$.
V	Nodes 1–6: 3-connected ($\kappa_3 = 3$); Nodes 7–12: 1-connected ($\kappa_1 = 1$); $\mathcal{W} = \mathcal{W}_1 \cup \mathcal{W}_3$.
VI	Nodes 1–6: 3-connected ($\kappa_3 = 3$); Nodes 7–12: 2-connected ($\kappa_2 = 2$); $\mathcal{W} = \mathcal{W}_2 \cup \mathcal{W}_3$.
VII	All sensor nodes are 3-connected ($\kappa_3 = 3$, $\mathcal{W}_3 = \{1, 2, \ldots, 12\}$), and $\mathcal{W} = \mathcal{W}_3$.

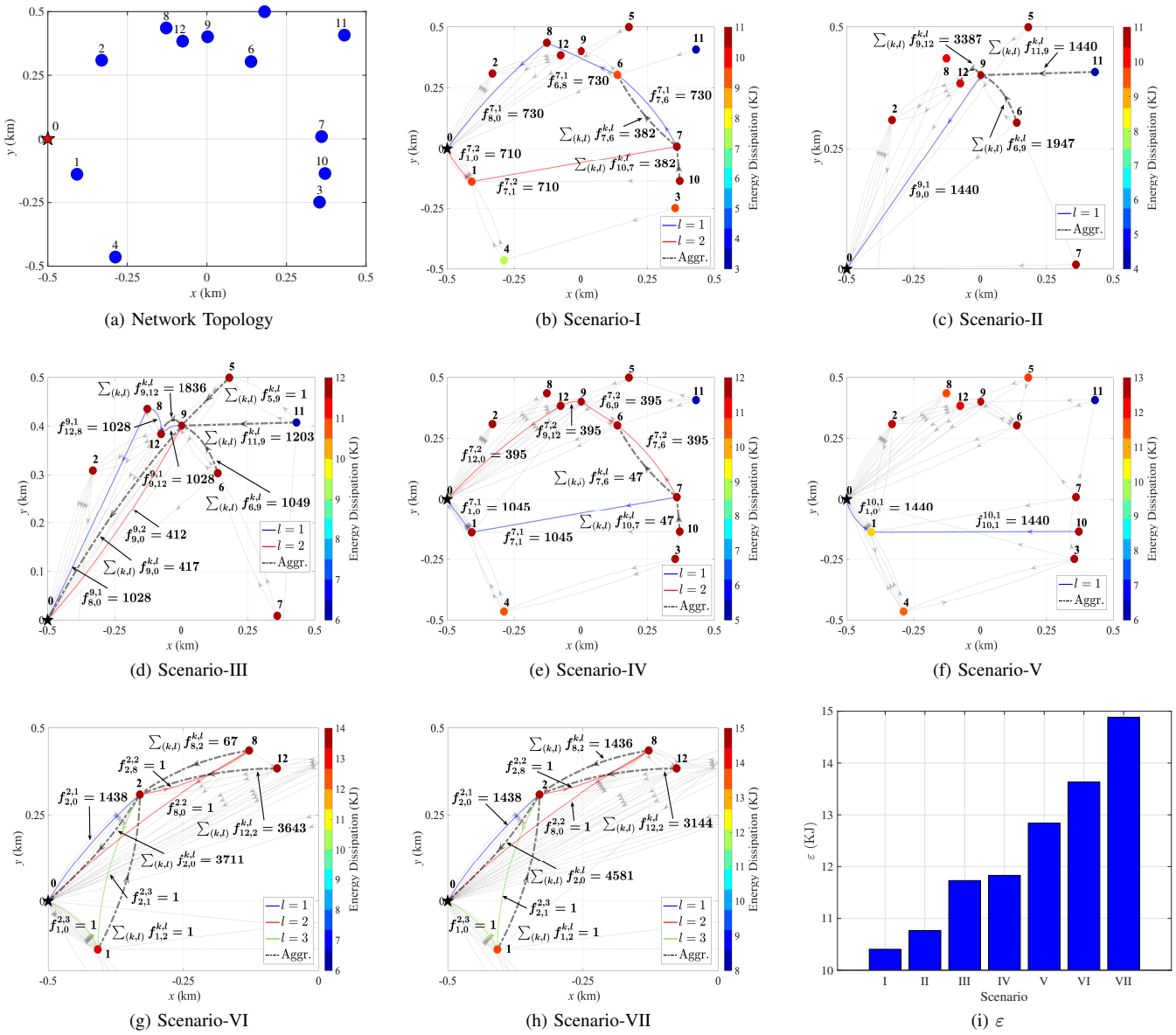

(a) Network Topology (b) Scenario-I (c) Scenario-II

(d) Scenario-III (e) Scenario-IV (f) Scenario-V

(g) Scenario-VI (h) Scenario-VII (i) ε

Fig. 3: Illustrations of packet flows and energy dissipation for a UWSN topology. (a) Network topology with node positions, where the BS is shown with a star and sensor nodes with disks. (b-h) data flows and node energy dissipation for seven non-uniform k-connectivity scenarios. (i) Maximum energy dissipation (ε) for the seven scenarios.

1 are 62.83 KJ, 76.61 KJ, and 121.96 KJ for the first, second, and third cases, respectively. Having characterized the impact of ξ on ε, in the rest of the analysis, we opt to utilize a single relative frequency value, which is $\xi = 1$.

B. Detailed Analysis of a UWSN Deployment

Although we utilized a deployment domain in the shape of a rectangular prism in the other subsections of this section, we employ a deployment topology in the form of a two-dimensional square area with dimensions of 1x1 km in this subsection, which can be considered as a cross section of rectangular prism because illustration of packet flows and node positions over a two-dimensional plane is more convenient. The BS, designated as node-0, is positioned at coordinates (-0.5, 0), while 12 sensor nodes are randomly distributed within the square network. The resulting topology and node coordinates are illustrated in Fig. 3a. Seven distinct scenarios, representing different k-connectivity configurations, are presented in Table III.

Figs. 3b to 3h show the solutions of the MILP model applied to the network topology for the seven non-uniform k-connectivity scenarios. For each scenario, the energy consumption of each sensor node is color encoded, where the numerical values of the colors are provided in the colored bars on the right-hand side of each subfigure. Across the investigated scenarios, different nodes exhibit the highest energy consumption. Specifically, node-7 consumes 10.40 KJ and 11.83 KJ in Scenarios I (Fig. 3b) and IV (Fig. 3e), respectively. Node-9 is the most energy-intensive node in Scenarios II (Fig. 3c) and III (Fig. 3d), with consumption levels of 10.77 KJ and 11.73 KJ, respectively. In Scenarios VI (Fig. 3g) and VII (Fig. 3h), node-2 exhibit the highest consumption, reaching 13.63 KJ and 14.88 KJ, respectively. In Scenario V (Fig. 3f) node-10 is the highest energy consumer (12.84 KJ).

Each sub-figure in Fig. 3 shows all flows generated by all nodes within the network with faint dashed lines. Moreover, we also highlight the paths connecting the node with the highest energy consumption to the BS, represented by blue (first path, $l = 1$), red (second path, $l = 2$), and green lines (third path, $l = 3$). For example, in Fig. 3b, node-7, identified as the node with the highest energy demand, transmits a total of 1440 packets to the BS, injecting 730 packets into its first path and 710 packets into the second. In addition, thick dashed gray lines depict the aggregated traffic flows (Aggr.) into and out of the highest-energy node when the node functions as a relay rather than a source. For example, in Fig. 3b, node-7 relays 382 packets incoming from node-10 to node-6.

Fig. 3i presents the optimal values of the objective function, ε, obtained from the MILP model for the scenarios. Energy dissipation of the highest energy consuming node in the network (ε) increases as the scenario number increases (i.e., from Scenarios I to Scenario VII). For example, ε values of Scenario II and Scenario VI are 10.77 KJ and 13.63 KJ, respectively. The main reason for such behavior is the increase in the number of disjoint paths in the network. For example, all sensor nodes in Scenario III are required to maintain at least two node-disjoint paths (i.e., there are at least 24 paths to be maintained in the UWSN) whereas in Scenario VII all sensor nodes are required to have three disjoint paths (i.e., at least 36 paths to be kept alive by control and data packet transmissions). It is possible to increase NetL by providing higher connectivity robustness to the most critical sensor nodes only. For example, ε values of Scenario V ($\kappa_1 = 1$, $\kappa_3 = 3$, and $|\mathcal{W}_1| = |\mathcal{W}_3| = 6$) and Scenario VII ($\kappa_3 = 3$ and $|\mathcal{W}_3| = 12$) are 12.84 KJ and 14.89 KJ, respectively (i.e., NetL of Scenario V is 15.97% higher than NetL of Scenario VII). However, performance gains in terms of NetL brought by non-uniform k-connectivity can be much higher in larger deployments as demonstrated in the next subsection.

TABLE IV: Energy dissipation of the highest energy consuming node (ε) for 11 non-uniform k-connectivity configurations (C#). Each row includes the cardinality of each connectivity set under consideration ($\kappa_1 = 1$ for $\mathcal{W}_1$, $\kappa_2 = 2$ for $\mathcal{W}_2$, and $\kappa_3 = 3$ for $\mathcal{W}_3$) with three UWSN deployment lengths ($dy =$ 1 km, 2 km, 3 km).

C#	$\lvert\mathcal{W}_1\rvert$	$\lvert\mathcal{W}_2\rvert$	$\lvert\mathcal{W}_3\rvert$	ε (KJ)		
				$dy = 1$ km	$dy = 2$ km	$dy = 3$ km
1	30	0	0	13.66	33.57	62.11
2	25	5	0	13.97	34.16	63.56
3	20	10	0	14.12	35.31	66.33
4	15	15	0	14.20	36.25	68.32
5	20	5	5	14.26	36.34	69.37
6	10	20	0	14.40	36.44	73.07
7	15	10	5	14.49	37.34	80.38
8	5	25	0	14.82	38.60	85.41
9	0	30	0	15.34	40.19	96.23
10	10	0	20	16.60	42.57	99.02
11	0	0	30	18.32	48.98	108.45

C. Analysis of Selected Larger Scale UWSN Configurations

In this subsection, we present a set of 11 selected UWSN deployment configurations to highlight the benefits of employing non-uniform k-connectivity in terms of ε. Each row of Table IV presents a distinct $\mathcal{W}_n$ configuration for three deployment volumes. Depth and width of the rectangular prism-shaped underwater deployment volume are kept constant while the length, d_y, is varied from 1 km to 3 km. Variation in length allow us to observe the impacts of higher average hop length from the sensor nodes to the BS. Different configurations have different sets of sensor nodes, however, the total number of sensor nodes in all configurations is kept constant ($|\mathcal{W}| = 30$). For example, in Configuration 7 there are 15 nodes in $\mathcal{W}_1$ (i.e., 15 predetermined sensor nodes are required to have at least one path to the BS), 10 nodes in $\mathcal{W}_2$ (i.e., 10 sensor nodes maintain at least two node-disjoint paths towards the BS), and 5 nodes in $\mathcal{W}_3$ (i.e., 5 sensor nodes have at least three paths to the BS). Sensor nodes are assigned to $\mathcal{W}_n$ sets randomly. Since we utilize a plurality of random topologies and set assignments, our results, which are statistical averages, characterize a more general case in comparison to a specific $\mathcal{W}_n$ set assignment scenario.

For each configuration, as the length of the deployment volume, d_y, increases, energy dissipation also increases. For example, in Configuration 4 ($|\mathcal{W}_1| = 15$ and $|\mathcal{W}_2| = 15$) ε values are 14.20 KJ, 36.25 KJ, and 68.32 KJ for $d_y =$ 1 km, $d_y = 2$ km, and $d_y = 3$ km, respectively. The reason for such increase is that the average length (in terms of both distance and hop count) of the paths from sensor nodes to the BS increases with the length of the deployment volume. The

energy consumption of sending packets to longer distances is higher in comparison to shorter distances. Another important observation is that the energy dissipation also increases with the average number of routing paths in UWSNs. For example, with a fixed deployment volume length ($d_y = 2$ km) ε for Configuration 2 (at least 35 paths to be maintained) and Configuration 8 (minimum 55 paths to be kept alive) are 34.16 KJ and 38.60 KJ, respectively. As such NetL of Configuration 2 is 13.00% larger than the NetL of Configuration 8 for $d_y = 2$ km.

It is possible to populate Table IV with many more configurations encompassing various sensor node-sets, however, the eleven configurations we present are sufficient to characterize the interplay between NetL and non-uniform k-connectivity assignment strategies. For example, with $d_y = 3$ km, NetL obtained with Configuration 11 (all sensor nodes are required to maintain 3 node-disjoint paths towards the BS) is 36.04% lower than the NetL obtained with Configuration 5 (only 5 sensor nodes are to keep 3 paths alive while 5 nodes are 2-connected and 20 nodes have only one path). Another insightful analysis can be gained by comparing Configuration 2 (only 5 nodes need to maintain 2-connectivity and the rest are required to have only one path towards the BS) and Configuration 9 (all sensor nodes are 2-connected) with $d_y = 3$ km, i.e., NetL of Configuration 2 is 51.40% higher than the NetL of Configuration 9.

D. Analysis of Probability of Node Survival

In this subsection, we analyze the probability of node survival under random node failures. For this analysis, we select Configuration 7 in Table IV ($|\mathcal{W}_1| = 15$, $|\mathcal{W}_2| = 10$, $|\mathcal{W}_3| = 5$, and $d_y = 1$ km). In each randomly generated topology, N_f nodes are randomly marked as failed, and we evaluate the percentage of the remaining nodes that remain connected to the BS. The probability of survival is then computed by averaging the survival rates across 20 randomly generated topologies. To enable a meaningful assessment of resilience across three connectivity levels, we handled the remaining nodes separately and evaluated their survival probabilities based on their initial connectivity (i.e., sensor nodes can forward their packets only over the original paths determined by the solution of the optimization model).

TABLE V: Probability of survival under random node failures.

N_f	Probability of survival		
	$k = 1$	$k = 2$	$k = 3$
1	0.92	1.00	1.00
2	0.86	0.99	1.00
3	0.80	0.98	1.00
4	0.74	0.96	0.99
5	0.70	0.94	0.99
6	0.65	0.92	0.98
7	0.62	0.90	0.97
8	0.58	0.88	0.95
9	0.55	0.86	0.94
10	0.52	0.84	0.92

Table V reveals that 3-connected nodes maintain connectivity with a probability of 0.92 despite one-third of the sensor nodes fail (i.e., $N_f = 10$). In comparison, 1-connected nodes remain connected with a probability of 0.52 under the same conditions. Note that probability of survival for 3-connected nodes with 3 node failures is 1.00, however, this is due to rounding of the results to two significant digits (i.e., the probability is, in fact, 0.998 with three significant digits).

V. Conclusion

Reliable connectivity and network lifetime are two important considerations for UWSNs. Uniform k-connectivity (i.e., all sensor nodes in the network are k-connected with a preset k value) guarantees that all sensor nodes in the network stay connected unless $k - 1$ of them cease functioning. However, k-connectivity comes with a prohibitively high cost in terms of network lifetime. As a remedy, in this study, we propose the novel concept of non-uniform k-connectivity for UWSNs (i.e., multiple node-sets with different connectivity levels coexist in the same network). Indeed, not all sensor nodes need the highest connectivity resilience, which is to be assessed by the requirements and priorities of the application under consideration. We created an MILP-based optimization framework to represent the energy consumption characteristics of non-uniform k-connectivity in UWSNs. We obtained the solutions of the optimization model for a wide range of scenarios, configurations, and parameters. Our results reveal that it is possible to increase UWSN lifetime more than 50.00% by providing the highest level of connectivity reliability to a select subset of sensor nodes instead of maintaining the same level of reliability for all sensor nodes in the network.

In this study, we explore the potential gains achievable by non-uniform k-connectivity in underwater environment. However, sensor network deployments in other environments, such as terrestrial deployments, can also benefit from non-uniform k-connectivity, which is a future research direction. Another interesting research avenue is to explore the impact of non-uniform k-connectivity in UWSNs with mobile BSs or with multiple static BSs.

References

[1] T. Qiu, Z. Zhao, T. Zhang, C. Chen, and C. L. P. Chen, "Underwater internet of things in smart ocean: System architecture and open issues," *IEEE Trans. Ind. Informat.*, vol. 16, no. 7, pp. 4297–4307, Jul. 2020.

[2] Y. Yuan, X. Zhuo, M. Liu, Y. Wei, and F. Qu, "A centralized cross-layer protocol for joint power control, link scheduling, and routing in UWSNs," *IEEE Internet Things J.*, vol. 11, no. 7, pp. 12 823–12 833, Apr. 2024.

[3] X. Wei, H. Guo, X. Wang, X. Wang, and M. Qiu, "Reliable data collection techniques in underwater wireless sensor networks: A survey," *IEEE Commun. Surveys Tuts.*, vol. 24, no. 1, pp. 404–431, Firstquarter 2022.

[4] H. U. Yildiz, V. C. Gungor, and B. Tavli, "Packet size optimization for lifetime maximization in underwater acoustic sensor networks," *IEEE Trans. Ind. Informat.*, vol. 15, no. 2, pp. 719–729, Feb. 2019.

[5] Z. A. Dagdeviren, V. K. Akram, O. Dagdeviren, B. Tavli, and H. Yanikomeroglu, "k-connectivity in wireless sensor networks: Overview and future research directions," *IEEE Netw.*, vol. 37, no. 3, pp. 140–145, May/Jun. 2023.

[6] M. Cobanlar, H. U. Yildiz, V. K. Akram, O. Dagdeviren, and B. Tavli, "On the tradeoff between network lifetime and k-connectivity based reliability in UWSNs," *IEEE Internet Things J.*, vol. 9, no. 23, pp. 24 444–24 452, Dec. 2022.

[7] M. Cobanlar, V. K. Akram, O. Dagdeviren, and B. Tavli, "Analysis of the tradeoff between network lifetime and k-connectivity in WSNs," in *Proc. Telecommun. Forum (TELFOR)*, 2018, pp. 1–4.

[8] M. S. Hegde and K. V. Santhosh, "Placement and interconnectivity in wireless sensor networks," in *Proc. Int. Conf. Artificial Intell. Comput. Electronics Commun. Syst. (AICECS)*, 2024, pp. 1–6.

[9] Z. Yun, X. Bai, D. Xuan, T. H. Lai, and W. Jia, "Optimal deployment patterns for full coverage and k-connectivity ($k \leq 6$) wireless sensor networks," *IEEE/ACM Trans. Netw.*, vol. 18, no. 3, pp. 934–947, Jun. 2010.

[10] A. Zrelli and T. Ezzedine, "A new approach of WSN deployment, k-coverage and connectivity in border area," *Wireless Pers. Commun.*, vol. 121, pp. 3365—-3381, Dec. 2021.

[11] A. Tripathi, H. P. Gupta, T. Dutta, R. Mishra, K. Shukla, and S. Jit, "Coverage and connectivity in WSNs: A survey, research issues and challenges," *IEEE Access*, vol. 6, pp. 26 971–26 992, Jun. 2018.

[12] S. T. Ozyer, B. Tavli, K. Dursun, and M. Koyuncu, "Systematic investigation of the effects of unidirectional links on the lifetime of wireless sensor networks," *Comput. Stand. Inter.*, vol. 36, no. 1, pp. 132–142, Nov. 2013.

[13] A. Aljughaiman, "Distributed node deployment algorithm using grid-based depth adjustable for UASNs," *Wireless Pers. Commun.*, vol. 138, pp. 189–227, Sept. 2024.

[14] H. Chen, C. Wu, M. Wu, B. Xu, and P. Fan, "Survey of connectivity restoration in 3D wireless ad hoc/sensor networks," *Int. J. Distrib. Sens. Netw.*, pp. 6 656 884:1–6 656 884:27, Apr. 2024.

[15] B. S. Panda and D. P. Shetty, "Minimum range assignment problem for two connectivity in wireless sensor networks," in *Proc. Int. Conf. Distrib. Comput. Internet Techn. (ICDCIT)*, 2014, pp. 122–133.

[16] H. Bagci, I. Korpeoglu, and A. Yazici, "A distributed fault-tolerant topology control algorithm for heterogeneous wireless sensor networks," *IEEE Trans. Parallel Distrib. Syst.*, vol. 26, no. 4, pp. 914–923, Apr. 2014.

[17] V. K. Akram, O. Dagdeviren, and B. Tavli, "A coverage-aware distributed k-connectivity maintenance algorithm for arbitrarily large k in mobile sensor networks," *IEEE/ACM Trans. Netw.*, vol. 30, no. 1, pp. 62–75, Feb. 2022.

[18] V. K. Akram and O. Dagdeviren, "DECK: A distributed, asynchronous and exact k-connectivity detection algorithm for wireless sensor networks," *Comput. Commun.*, vol. 116, pp. 9–20, Jan. 2018.

[19] O. Dagdeviren and V. K. Akram, "PACK: Path coloring based k-connectivity detection algorithm for wireless sensor networks," *Ad Hoc Netw.*, vol. 64, pp. 41–52, Jun. 2017.

[20] M. R. Henzinger, S. Rao, and H. N. Gabow, "Computing vertex connectivity: New bounds from old techniques," *J. Algorithms*, vol. 34, no. 2, pp. 222–250, Feb. 2000.

[21] A. Cornejo and N. Lynch, "Fault-tolerance through k-connectivity," in *Proc. Workshop Netw. Sci. Sys. Issues Multirobot Autonomy (ICRA)*, vol. 2, 2010, pp. 1–4.

[22] M. Jorgic, N. Goel, K. Kalaichevan, A. Nayak, and I. Stojmenovic, "Localized detection of k-connectivity in wireless ad hoc, actuator and sensor networks," in *Proc. Int. Conf. Comput. Commun. Netw. (ICCCN)*, 2007, pp. 33–38.

[23] O. Dagdeviren, V. K. Akram, and B. Tavli, "Design and evaluation of algorithms for energy efficient and complete determination of critical nodes for wireless sensor network reliability," *IEEE Trans. Rel.*, vol. 68, no. 1, pp. 280–290, Mar. 2019.

[24] A. Vavoulas, H. G. Sandalidis, and D. Varoutas, "Underwater optical wireless networks: A k-connectivity analysis," *IEEE J. Ocean. Eng.*, vol. 39, no. 4, pp. 801–809, Oct. 2014.

[25] S. Lee, M. Younis, and M. Lee, "Connectivity restoration in a partitioned wireless sensor network with assured fault tolerance," *Ad Hoc Netw.*, vol. 24, pp. 1–19, Jan. 2015.

[26] V. K. Akram, O. Dagdeviren, and B. Tavli, "Distributed k-connectivity restoration for fault tolerant wireless sensor and actuator networks: algorithm design and experimental evaluations," *IEEE Trans. Rel.*, vol. 70, no. 3, pp. 1112–1125, Sept. 2021.

[27] W. Mo, D. Qiao, and Z. Wang, "Lifetime maximization of sensor networks under connectivity and k-coverage constraints," in *Lecture Notes in Computer Science (Proc. Distributed Computing in Sensor Systems – DCOSS)*, P. Gibbons, T. Abdelzaher, J. Aspnes, and R. Rao, Eds. Berlin, Heidelberg: Springer, 2006, vol. 4026, pp. 422–442.

[28] M. A. Khan, N. Javaid, A. Majid, M. Imran, and M. Alnuem, "Dual sink efficient balanced energy technique for underwater acoustic sensor networks," in *Proc. Int. Conf. Adv. Inform. Netw. Appl. Work. (WAINA)*, 2016, pp. 551–556.

[29] H. Xu, F. Ye, H. Su, and C. Su, "Energy-efficient relay selection and power allocation optimization for lifetime maximization in underwater acoustic sensor networks," *IEEE Sens. J.*, vol. 25, no. 11, pp. 20 854–20 869, May 2025.

[30] J. Zhu, K.-L. Hung, and B. Bensaou, "Tradeoff between network lifetime and fair rate allocation in wireless sensor networks with multi-path routing," in *Proc. ACM Int. Symp. Model. Anal. Simul. Wirel. Mobile Syst. (MSWiM)*, 2006, pp. 301–308.

[31] T. Bektas and L. Gouvei, "Requiem for the Miller–Tucker–Zemlin subtour elimination constraints?" *Eur. J. Oper. Res.*, vol. 236, no. 3, pp. 820–832, Aug. 2014.

[32] M. Cheng, X. Gong, and L. Cai, "Joint routing and link rate allocation under bandwidth and energy constraints in sensor networks," *IEEE Trans. Wirel. Commun.*, vol. 8, no. 7, pp. 3770–3779, Jul. 2009.

[33] L. Gurobi Optimization, *Gurobi Optimizer Reference Manual*, 2025. [Online]. Available: https://www.gurobi.com

Cagla Tantur Karagul received the B.Sc. and M.Sc. degrees in Electrical and Electronics Engineering from Middle East Technical University, Ankara, Turkiye in 2015 and TOBB University of Economics and Technology, Ankara, Turkiye, in 2017, respectively. She is currently pursuing her Ph.D. in Electrical and Electronics Engineering at TOBB University of Economics and Technology, Ankara, Turkiye. Her research interests include computer networks, wireless communications, and optimization.

Mehmet Burak Akgun holds B.Sc., M.Sc. and Ph.D. degrees in Electrical and Electronics Engineering from Middle East Technical University, Ankara, Turkiye in 2008; TOBB University of Economics and Technology, Ankara, Turkiye in 2010 and Computer Science and Engineering, University of Nevada Reno, USA in 2014, respectively. He is an assistant professor of Computer Engineering at TOBB University of Economics and Technology, Ankara, Turkiye. His research interests are in big data, machine learning and network science.

Huseyin Ugur Yildiz received the B.Sc. degree from Bilkent University, Ankara, Turkiye, in 2009; the M.Sc. and Ph.D. degrees from TOBB University of Economics and Technology, Ankara, Turkiye, in 2013 and 2016, respectively, all in Electrical and Electronics Engineering. He is an associate professor in the department of Electrical and Electronics Engineering at TED University, Ankara, Turkiye. His research focuses on the applications of optimization techniques for modeling and analyzing research problems on underwater wireless sensor networks.

Bulent Tavli is currently a professor with the department of Electrical and Electronics Engineering, TOBB University of Economics and Technology, Ankara, Turkiye. His research interests include data analytics, machine learning, quantum computing, network science, wireless communications and networks, algorithm design and analysis, and optimization.